J. Synchrotron Rad. (1999). **6**, 1125–1132

X-ray magnetic circular dichroism with tunable polarization helicity

L. Varga,[a] C. Giles,[b] Y. L. Zheng,[a] S. Pizzini,[c] F. de Bergevin,[d] A. Fontaine[c] and C. Malgrange[a]*

[a]Laboratoire de Minéralogie-Cristallographie, Universités Paris 6 et Paris 7, Associé au CNRS, Case 115, 75252 Paris CEDEX 05, France, [b]Instituto de Física 'Gleb Wataghin', Universidade Estadual de Campinas, CP 6165, 13083-970 Campinas-SP, Brazil, [c]Laboratoire Louis Néel, CNRS, BP 166, 38042 Grenoble CEDEX, France, and [d]Laboratoire de Cristallographie, CNRS, BP 166, F-38042 Grenoble CEDEX, France. E-mail: malgrang@lmcp.jussieu.fr

(*Received 11 June 1999; accepted 31 August 1999*)

X-ray magnetic circular dichroism spectra have previously been obtained by switching the polarization helicity with a diamond quarter-wave plate (QWP) and keeping the applied magnetic field on the sample as an independent variable [Giles, Malgrange, Goulon, de Bergevin, Vettier, Fontaine, Dartyge & Pizzini (1994). *Nucl. Instrum. Methods*, A**349**, 622–625]. These results were obtained by subtracting an undesirable non-magnetic residual spectrum. Experiments reported here show that this residual spectrum mainly originates from a slight lateral displacement of the forward-diffracted beam in the QWP. A quantitative analysis of the phenomenon is in good agreement with predictions from X-ray dynamical theory.

Keywords: X-ray magnetic circular dichroism; X-ray phase plates; X-ray polarization.

1. Introduction

The use of polarized X-rays for the study of microscopic properties of magnetic materials has become popular with the development of two new experimental techniques using synchrotron radiation tuned to the absorption edges of the magnetic atoms. Resonant magnetic X-ray scattering or RMXS (de Bergevin & Brunel, 1972; Gibbs *et al.*, 1988; Vettier, 1994) probes the real part of the index of refraction through scattering whereas X-ray magnetic circular dichroism or XMCD (Schütz *et al.*, 1989; Chen *et al.*, 1990; Dartyge *et al.*, 1992) probes its imaginary part. Both techniques have the advantage of being element- and orbital-specific.

In this paper we will concentrate on the development of an experimental technique improving the capabilities of recording XMCD spectra in the energy-dispersive mode. The X-ray magnetic circular dichroic signal is defined as the difference in absorption for right- and left-handed circularly polarized X-rays by a magnetic sample with the magnetization direction along the photon wavevector. XMCD spectra are generally recorded keeping the polarization helicity constant and reversing the sample magnetization direction by means of an external magnetic field. If one uses a quarter-wave plate (QWP) to transform the linear polarization into circular polarization it is easy to reverse the helicity of the outgoing circular polarization and then to go back to the original definition of the XMCD. Note that in third-generation sources this can be easily performed using helical undulators.

X-ray quarter-wave plates adapted to an energy-dispersive absorption spectrometer have been developed and used for recording XMCD spectra in the 7–11 keV energy range on the DCI synchrotron ring at LURE, Orsay, France (Giles, Malgrange, Goulon, de Bergevin, Vettier, Dartyge *et al.*, 1994). The first XMCD spectra recorded by flipping the polarization helicity of the incoming beam (Giles, Malgrange, Goulon, de Bergevin, Vettier, Fontaine *et al.*, 1994) are presented in Fig. 1. They were measured at the L_3 edge of holmium ($E_0 = 8071$ eV) for an $HoFe_2$ Laves phase sample. The spectra obtained for a magnetic field parallel (Fig. 1*a*) and antiparallel (Fig. 1*b*) to the photon wavevector are not exactly opposite, as they would be if XMCD was the only contribution to the signal. If we admit that the signal derives from XMCD plus an additional non-magnetic spectrum R, the XMCD can be obtained from the half-difference of spectra (*a*) and (*b*) (Fig. 1*c*), and R from their half-sum (Fig. 1*d*). The XMCD obtained in this way is identical to that obtained by reversing the direction of the magnetic field. The advantage of this method is that the magnetic field becomes a variable parameter: XMCD spectra can be measured as a function of magnetic field intensity and, for example, element-selective hysteresis cycles can be measured (Pizzini *et al.*, 1997).

The origin and behaviour of such a residual spectrum has not been understood in detail until now. The series of

experiments reported in this paper were performed later in order to analyse the residual spectrum, whose origin is now fully understood.

This paper is organized as follows. In §2 we briefly describe the concept of the energy-dispersive spectrometer used to record XMCD with an X-ray quarter-wave plate. §3 recalls the principle of the quarter-wave plate. In §4 we present experiments which show that two effects are combined to give the residual signal; one is due to the imperfections present in the crystal and the other results from a displacement of the beam analysed using dynamical theory of X-ray diffraction in §5.

2. XMCD on an energy-dispersive spectrometer

Measurements were carried out on the energy-dispersive absorption beamline at DCI-LURE (D11).

The principle of the energy-dispersive spectrometer has already been described in detail elsewhere (Tolentino *et al.*, 1988) and will be briefly recalled here. The energy-dispersive set-up uses a curved crystal optics to focus a polychromatic beam onto the sample position coupled to a one-dimensional detector (linear array of 1024 diodes, each 25 μm) allowing the full spectra to be recorded at once. The polychromatic beam has an energy–angle correlation that is transformed into an energy–position correlation on the detector. This allows the full spectra to be obtained without any mechanical movement, *i.e.* with great stability.

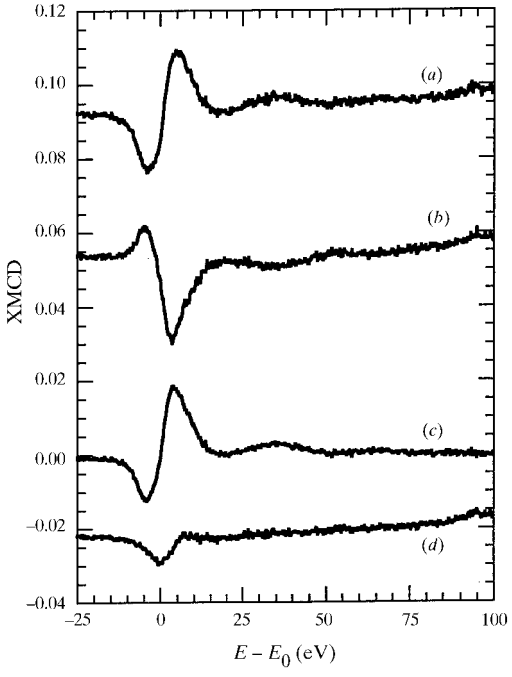

Figure 1
XMCD spectra at the Ho L_3 absorption edge (E_0) of an $HoFe_2$ sample obtained by switching the polarization helicity with a quarter-wave plate. (*a*) Spectrum obtained with a constant magnetic field parallel to the photon wavevector; (*b*) spectrum obtained with the magnetic field antiparallel to the photon wavevector; (*c*) pure XMCD signal without artifacts obtained as the half-difference of spectra (*a*) and (*b*); (*d*) pure residual spectrum *R* obtained as the half-sum of (*a*) and (*b*).

Circularly polarized X-rays can be obtained either from the source (bending magnet or exotic insertion devices) or by transforming the linear polarization state of the incoming beam by a quarter-wave plate. X-ray quarter-wave plates are based on the use of crystal plates near a Bragg diffraction condition (Giles *et al.*, 1993). When such a device is used in the energy-dispersive spectrometer a non-dispersive configuration between the crystal phase plate and the curved crystal polychromator has to be fulfilled in order to simultaneously transform the entire energy bandwidth from linear to circular polarization. This is performed taking into account the fact that the diffraction plane of the quarter-wave plate is set at an angle $\psi = 45^\circ$ from the horizontal plane to allow equal amplitudes of σ and π polarizations in the incoming beam. It has been demonstrated that a careful change of the diffraction plane around the 45° value is essential to fulfill the non-dispersive condition which is given by

$$\tan\theta_2/\tan\theta_1 = 2\cos\psi(1 - qb/p)^{-1}, \qquad (1)$$

where θ_1 and θ_2 are the Bragg angles on the curved polychromator and the phase plate, respectively, for the mean energy, b is the asymmetry factor related to the angle of asymmetry α of the reflecting planes in the curved polychromator given by $b = \sin(\theta - \alpha)/\sin(\theta + \alpha)$, p is the distance between the source and the crystal and q is the distance between the crystal and the focus point.

Let us call d_1 and d_2 the lattice plane distances relative to the reflections on the curved Si crystal and the QWP. This condition allows d_1/d_2 and the angle ψ between the two planes of diffraction to be determined for a given mean energy. A 111 reflection on the curved silicon crystal and a 111 reflection on the diamond crystal are a good combination which give angles $\psi \simeq 45^\circ$ for X-ray energies between 7 and 15 keV. Details of such arrangements are described by Giles, Malgrange, Goulon, de Bergevin, Vettier, Dartyge *et al.* (1994).

The energy-dispersive set-up has unique advantages when using a quarter-wave plate to record XMCD spectra. First, the QWP is already set for the whole energy range of the XMCD spectra and does not need further angular adjustments. This improves the stability of the set-up and allows measurements of very small dichroic signals. Second, the QWP allows a fast tunability of the polarization helicity of the beam enabling a wide range of experiments in the study of magnetic materials. The principle of the X-ray quarter-wave plate in the transmission mode as used in this work will now be revised.

3. Principle of the QWP

The X-ray quarter-wave plates principle relies on the birefringence of perfect crystals close to Bragg diffraction incidence. Several set-ups are possible with different efficiencies and X-ray energy ranges of application. The

quarter-wave plate in the transmission mode (*i.e.* selecting the forward-diffracted beam) used in this work was first proposed by Dmitrienko & Belyakov (1980) and experimentally evidenced using a very well collimated beam by Hirano *et al.* (1991). The phase shift induced by the phase plate varies with the angle of incidence of the beam on the plate and can be set equal to $\pi/2$ or $-\pi/2$ by a simple rotation of the phase plate. Starting with incoming linear polarization one can then obtain circular polarization with tunable helicities.

X-ray dynamical theory (Authier, 1961, 1986) shows that there is a difference between σ and π polarization indices of refraction, denoted by n_σ and n_π, respectively (Malgrange, 1996). This difference is maximum inside the domain of reflection but it decreases rather slowly outside this domain where the phase shift induced by a plate is given to a very good approximation by

$$\varphi = (2\pi/\lambda)(n_\sigma - n_\pi)t = -At/\Delta\Theta, \qquad (2)$$

with $A = r_e^2(F_h F_{\bar{h}})\lambda^3 \sin 2\theta_B/2\pi V^2$.

$\Delta\Theta$, called the offset, is the difference between the angle of incidence and the incidence at the middle of the rocking curve. It is often written as $\Delta\Theta = \Delta\theta - \Delta\theta_0$, where $\Delta\theta$ is the departure from exact Bragg incidence and $\Delta\theta_0 = \chi_0(1/b - 1)/(2\sin 2\theta_B)$, t is the beam path far from Bragg diffraction, b is the asymmetry factor defined in §2, r_e is the classical electron radius and F_h is the structure factor.

From equation (2) the hyperbolic dependence of the phase shift with the angular offset can be observed. The factor A multiplied by the beam path of X-rays through the crystal determines the angular position that fulfills a 90° phase shift between the σ and π components of the beam. In order to change the sign of the phase shift, and consequently the helicity of the circular polarization, a simple rotation of the crystal from positive to negative values of the offset is necessary. The birefringence is the same for the diffracted and the forward-diffracted beam. It is then very convenient to use, as shown in this work, the forward-diffracted beam which does not change the direction of the beam.

It is also convenient to have an offset value, corresponding to the 90° phase shift, well outside the domain of reflection. Within the reflection domain differences in the transmission profiles for the σ and π components decrease the ellipticity of the transmitted beam. Also, the rate of change of the phase shift φ is quite large increasing the sensitivity of the quarter-wave plate to the divergence of the incident beam. Furthermore, far from the reflection domain only one wavefield is excited and thus either the Laue or Bragg geometry can be used.

The value of the offset that corresponds to a phase shift of 90° can be increased by increasing either the A value or the value of the beam path t [equation (2)]. A is defined by the X-ray energy and the reflection on the QWP crystal. The beam path can be increased keeping a compromise with the transmission through the QWP. This is better achieved using crystals with a low absorption coefficient and this is the reason for using diamond rather than silicon crystals.

For a crystal of given thickness, the beam path t inside the crystal depends on the geometry of the reflection. Here the diamond QWP is a (111) plate, 0.72 mm thick, and a $11\bar{1}$ reflection is used in Laue asymmetric geometry. The angle α between the normal to the crystal surface and the incident beam is 19.47° and we chose to use the smaller beam path which corresponds to a beam path almost normal to the crystal surface since the Bragg angle for the 111 reflection on diamond at the Ho L_3 edge (λ = 1.536 Å) is equal to 21.9°. Under these conditions the value of the offset satisfying equation (2) for a phase shift equal to $\pi/2$ is −43 arcsec. Owing to the divergence of the incident beam, the offset giving the maximum value of the circular polarization rate is larger. For a Gaussian incident beam of FWHM 75 arcsec, the theoretical value is −74 arcsec with a flat maximum. The spectra shown in Figs. 1(*a*) and 1(*b*) were taken for non-exactly symmetric offsets of the order of 60–70 arcsec.

4. Measurement of XMCD flipping the polarization helicity

4.1. *Experimental procedure*

The usual procedure of recording an XMCD signal flipping the polarization helicity is to identify the positive and negative offset values ($\Delta\Theta_1$ and $\Delta\Theta_2$) of the QWP that produce the highest XMCD signals. These values correspond to the maximum of right- and left-handed circular polarizations. Then the experimental spectrum is recorded as the difference of the absorption spectra obtained with the QWP set at these two offset values keeping the external magnetic field constant.

Previous typical results shown in Fig. 1 [curves (*a*) and (*b*)] show that the recorded spectrum has an additional signal to the XMCD signal. A clear understanding of the origin of the residual spectrum can be obtained from a detailed analysis of the recording procedure. Let us denote the absorption coefficient and thickness of the QWP and the sample by μ_q, t_q and μ_s, t_s, respectively, and let I_0, I_q and I_s be the intensities at the exit of the curved polychromator, after the QWP and after the sample, respectively (Fig. 2).

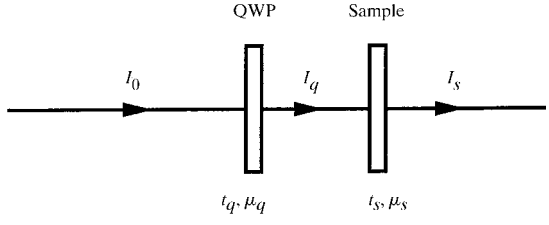

Figure 2
Schematic drawing defining the notation used in the text. I_q is the intensity after the QWP, t_q and μ_q are the thickness and absorption coefficient of the QWP. I_s is the intensity after the sample and t_s and μ_s are the thickness and absorption coefficient of the sample, respectively.

Then the transmitted intensities I_q and I_s can be expressed by

$$I_q(\Delta\Theta) = I_0 \exp[-\mu_q(\Delta\Theta)t_q]$$

$$I_s(\Delta\Theta) = I_q(\Delta\Theta) \exp[-\mu_s(\Delta\Theta)t_s]$$

where μ_q, μ_s, I_q and I_s have been explicitly written as functions of $\Delta\Theta$ to evidence their dependence on the angular offset of the QWP. The dependence of μ_s on $\Delta\Theta$ is related to its variation with the sign and amplitude of the circular polarization rate produced by the QWP at offset $\Delta\Theta$. The dependence of μ_q on $\Delta\Theta$ will be discussed in §4.2.

For the spectrum recorded without the sample, *i.e.* after the quarter-wave plate only, then

$$\ln[I_q(\Delta\Theta_1)] - \ln[I_q(\Delta\Theta_2)] = \mu_q(\Delta\Theta_2)t_q - \mu_q(\Delta\Theta_1)t_q = M, \quad (3)$$

and, for the signal after the QWP and the sample,

$$\ln[I_s(\Delta\Theta_1)] - \ln[I_s(\Delta\Theta_2)] = [\mu_q(\Delta\Theta_2)t_q - \mu_q(\Delta\Theta_1)t_q] + [\mu_s(\Delta\Theta_2)t_s - \mu_s(\Delta\Theta_1)t_s] = M + N, \quad (4)$$

where $N = \mu_s(\Delta\Theta_2)t_s - \mu_s(\Delta\Theta_1)t_s$.

Equation (4) shows that the XMCD spectrum is the sum of two signals: N due to the magnetic sample and proportional to the dichroic signal, and M from the difference in the absorption coefficient of the QWP for two different offset values.

In order to isolate the artifacts in the spectrum solely due to the diamond phase retarder, two series of absorption spectra were recorded, one with a non-magnetic sample containing holmium, $HoCo_2$, the other without any sample. The 'XMCD-like' spectra were recorded flipping the QWP between a constant large negative offset $\Delta\Theta_{ref}$ = −300 arcsec where the artifacts become negligible and several values of the offset $\Delta\Theta$ including $\Delta\Theta$ = 0 where X-ray dynamical effects are maximum. These spectra are referred to later as $Sp_J(\Delta\Theta)$,

$$Sp_J(\Delta\Theta) = \ln I_J(-300\,\text{arcsec}) - \ln I_J(\Delta\Theta),$$

where $J = Q$ without the sample [equation (3)] and $J = S$ [equation (4)] with the non-magnetic $HoCo_2$ sample.

Fig. 3 shows different $Sp_Q(\Delta\Theta)$ recorded with the QWP only. A clear variation of the transmitted intensity through the QWP as a function of the angular offset $\Delta\Theta$ is evidenced. This signal corresponds to the term M in equation (3) and its origin will be discussed in §4.2.

Subtracting this signal from the signal recorded with a sample should result in an XMCD signal for a magnetic sample or no signal for a non-magnetic sample. The presence of a signal in the difference spectra recorded with a non-magnetic sample is due to an artifact created by the transmission of the beam through the sample and will be analysed in §4.3.

4.2. *Influence of the diamond phase plate*

The spectra shown in Fig. 3, obtained with the QWP only, present two main features. First, their mean value varies with $\Delta\Theta$ and, second, some of them present rather large local variations around this mean value.

The mean value variation originates from the transmission profile of the QWP. The full line in Fig. 4 represents the transmission curve calculated for a perfect diamond crystal with a diffraction plane at ψ = 42.4° from the horizontal plane and convoluted by a Gaussian function of FWHM 75 arcsec representing the monochromatic divergence of the beam as found by other independent measurements (Giles, 1995).

The mean value of the different $Sp_Q(\Delta\Theta)$ is plotted in Fig. 4 by reference to the transmitted intensity at $\Delta\Theta_{ref}$ =

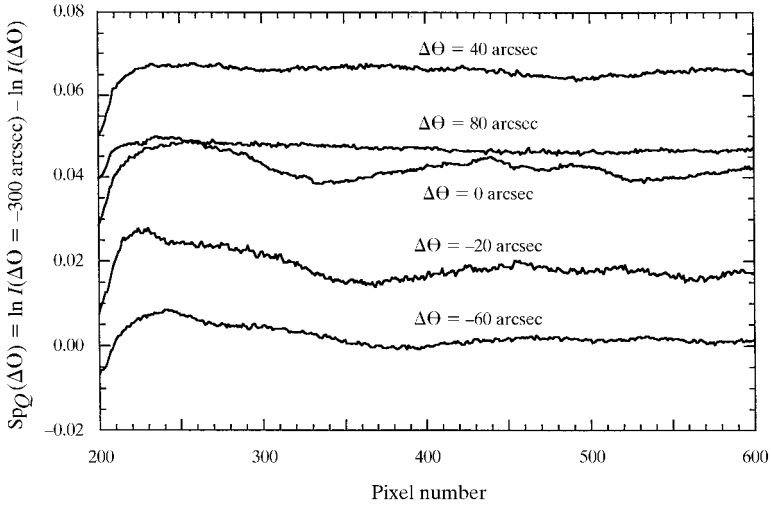

Figure 3
Spectra $Sp_Q(\Delta\Theta)$ recorded without the sample by flipping the QWP between a constant large negative offset of −300 arcsec and several $\Delta\Theta$ values (−60, −20, 0, 40 and 80 arcsec).

−300 arcsec. The agreement is quite good, in view of the fact that the diamond QWP is a good but non-perfect crystal.

In the energy-dispersive set-up the QWP, positioned typically 50 cm from the focus point, is crossed by a divergent X-ray beam. X-rays with different energies traverse different regions of the QWP crystal. In the case of a non-ideally perfect crystal these different regions may have slight misorientations inducing local changes of the offset value, which can create variations in the transmitted intensity. This explains the oscillations particularly enhanced in the spectra for $\Delta\Theta = 0$ arcsec and $\Delta\Theta = -20$ arcsec (Fig. 3).

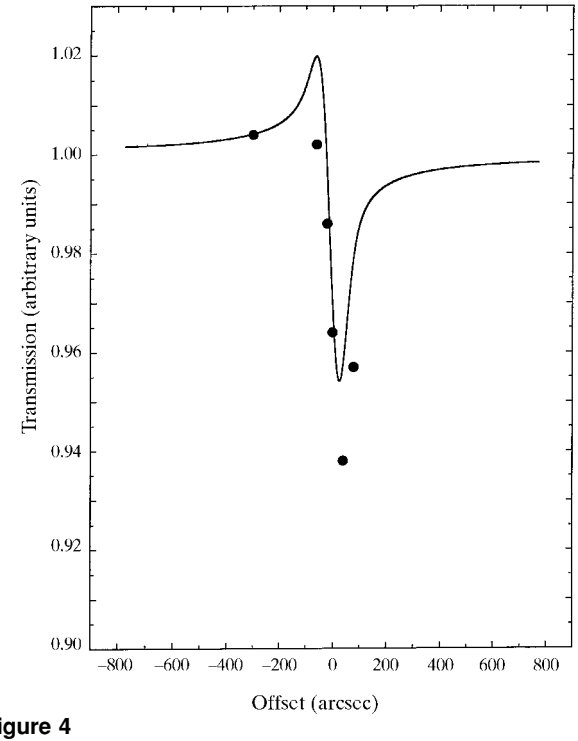

Figure 4
Calculated transmission profile (full line) of a perfect diamond crystal, 111 reflection in asymmetric Laue geometry with a diffraction plane inclined by $\psi = 42.4°$ with respect to the horizontal linear polarization direction of the incident beam, convoluted by a Gaussian profile of FWHM 75 arcsec. The filled circles represent the transmitted mean value of the QWP for different offsets $\Delta\Theta$ by reference to the transmission for $\Delta\Theta = -300$ arcsec.

To check that the observed variations of the signal are due to crystal defects, the crystal was translated horizontally (towards lower energies) to change the spectral bandwidth illuminating a given part of the crystal. As expected, the main features of the spectrum were also translated towards lower energies.

Thickness inhomogeneities of the QWP may also provoke different transmitted intensities in different regions of the spectrum.

4.3. *Evidence of a lateral translation of the beam*

In §5 we will demonstrate that the mean position of the X-ray beam on the exit surface of the crystal varies with the offset. The incident beam arrives on the QWP at point O (Fig. 8) and would exit at A if the propagation was straight. In fact, the beam exits at A' whose position depends on $\Delta\Theta$. The forward-diffracted beam leaves the crystal parallel to the incident beam but shifted by a length noted $x(\Delta\Theta)$.

In this section we will analyse the effects of such a displacement on the difference of two absorption spectra measured for two different offsets. Let us call Δx the lateral shift of the beam when going from one offset, $\Delta\Theta_1$, to the other, $\Delta\Theta_2$. It gives the same displacement on the linear detector which is set perpendicular to the beam. A variation of position on the detector is equivalent to a shift in energy. The difference of the two spectra therefore gives

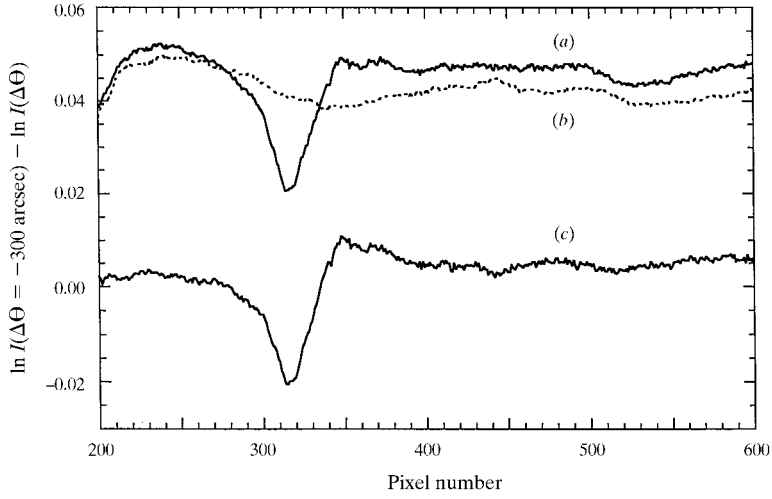

Figure 5
(*a*) Spectrum $Sp_S(\Delta\Theta = 0)$ recorded with a non-magnetic sample containing Ho ($HoCo_2$) by flipping the QWP between a constant and large negative offset $\Delta\Theta_{ref} = -300$ arcsec and $\Delta\Theta = 0$ arcsec. (*b*) Spectrum $Sp_Q(\Delta\Theta = 0)$ recorded without the sample. (*c*) Signal obtained as the difference between spectra (*a*) and (*b*).

rise to a derivative signal. Let us call $\mu_s' t_s$ the spectrum measured for the $\Delta\Theta_1$ offset and $\mu_s t_s$ for $\Delta\Theta_2$. Then,

$$\mu_s' t_s - \mu_s t_s = \frac{\partial(\mu_s t_s)}{\partial x}\Delta x. \tag{5}$$

$\partial(\mu_s t_s)/\partial x$ represents the derivative of the absorption signal with respect to the coordinate x along the linear detector. This is proportional to the derivative with respect to the energy E and is maximum at the absorption edge.

A lateral displacement Δx therefore produces a signal which is proportional to the lateral displacement itself and to the derivative of the absorption spectrum. This will appear as a pseudo-dichroic signal.

In order to evidence this effect we have chosen a non-magnetic sample $HoCo_2$, at room temperature, for which XMCD does not contribute to the difference signal.

From each spectrum $Sp_S(\Delta\Theta)$ recorded for the $HoCo_2$ sample we subtracted the spectrum $Sp_Q(\Delta\Theta)$ obtained with the QWP only (Figs. 5*a* and 5*b*). The result (Fig. 5*c*) was then compared with a signal proportional to the derivative of the absorption signal (dotted line in Fig. 6*a*).

From the coefficient of proportionality one can deduce the value of the displacement of the beam on the array of diodes [equation (5)]. For the case $\Delta\Theta = 0$ the displacement of the beam has been determined to be equal to 17.5 μm.

The same comparison for the case $\Delta\Theta = -20$ arcsec gives a displacement of the beam equal to 11 μm (Fig. 6*b*).

The different values of the displacements thus determined have been plotted as a function of $\Delta\Theta$ in Fig. 7. The experimental results show a dependence of the displacement on the offset having its maximum at the centre of the reflection domain. It will be shown below that this is in agreement with dynamical theory.

5. Dynamical theory effect on XMCD spectra

In the case of Bragg diffraction in transmission geometry (Laue case) in a perfect crystal, an incident beam with an offset $\Delta\Theta$ gives rise to two wavefields 1 and 2 each of which propagates in a direction given by its Poynting vector $\mathbf{P}_j$ (j = 1, 2) expressed by

$$\mathbf{P}_j = \mathbf{s}_0|D_{0j}^2| + \mathbf{s}_h|D_{hj}^2|,$$

where $\mathbf{s}_0$ and $\mathbf{s}_h$ are unit vectors in the incident and reflected directions, respectively, and D_{hj} and D_{0j} are the amplitudes of the diffracted and the forward-diffracted wave, respectively.

Let us consider an incident beam impinging the crystal at point O (Fig. 8). The incident direction intersects the exit surface of the crystal at point A, and the Poynting vector $\mathbf{P}_j$ issued from O intersects the exit surface at point P_j. Let us call M the middle of the basis of the Borrmann fan OAB and X_j the ratio $\overline{MP_j}/\overline{MA}$. Straightforward geometrical considerations lead to a very simple formula for X_j given below,

$$X_j = \overline{MP}_j/\overline{MA} = (1 - R_j)/(1 + R_j),$$

where $R_j = |\gamma_h/\gamma_0|(|D_{hj}{}^2|/|D_{0j}{}^2|)$, γ_0 and γ_h are the cosines of the angles ψ_0 and ψ_h between the normal to the crystal surface and the incident and reflected direction, respectively. Let us mention that the asymmetry factor b defined in §2 is equal to γ_0/γ_h.

The expression for R_j is very simple when expressed as a function of the usual dimensionless parameter η defined by

$$\eta = (\Delta\Theta \sin 2\theta)/[|C|(|\gamma_h|/\gamma_0)^{1/2}(\chi_h\chi_{\bar{h}})^{1/2}],$$

with $\chi_h = -\lambda^2 F_h r_e/\pi V$, so that,

$$R_j = |\chi_h/\chi_{\bar{h}}||(\eta^2 + 1)^{1/2} \pm \eta|^2,$$

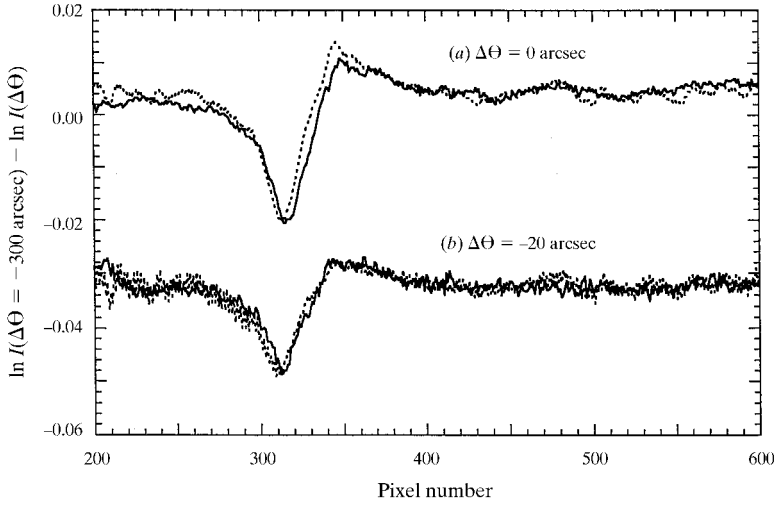

Figure 6
(*a*) Full line: $Sp_S(\Delta\Theta = 0) - Sp_Q(\Delta\Theta = 0)$ shown also in Fig. 5(*c*). Dotted line: derivative of the absorption spectrum of the same $HoCo_2$ sample multiplied by a factor corresponding to a displacement of the beam of 17.5 μm. (One pixel corresponds to 25 μm.) (*b*) Same as (*a*) for $\Delta\Theta = -20$ arcsec and the multiplying factor corresponds to a 11 μm displacement.

where the positive (negative) sign holds for wavefield 1 (wavefield 2).

When X_j is known it is possible to calculate the distance P_jQ (Fig. 8) defined as the distance from P_j to OA which is the incident beam direction. Let us call x_j the distance P_jQ, which can be written as,

$$x_j = \cos\psi_0(\tan\psi_0 + \tan\psi_h)(e/2)(1 - X_j),$$

where e is the thickness of the QWP.

In order to calculate the correct displacement of the beam in the set-up described here we have to take into account the rather large divergence of the incident beam due to the size of the source. The incident intensity I_0 is assumed to have a Gaussian angular distribution $I_0(\Delta\Theta - \Delta\Theta_m)$ centred around the mean offset $\Delta\Theta_m$. For each offset the two wavefields propagate giving rise to forward-diffracted waves with an intensity $I_{0j}(\Delta\Theta) = |D_{0j}(\Delta\Theta)|^2$ where

$$D_{0j} = [(\eta^2+1)^{1/2} - (\pm\eta)]/[2(\eta^2+1)^{1/2}]\exp(-i\pi k\chi_0 z/\gamma_0) \times \exp\{-i\pi z/\Lambda[\eta \pm (\eta^2+1)^{1/2}]\}$$

where $\Lambda = \lambda(\gamma_0|\gamma_h|)^{1/2}/(\chi_h\chi_{\bar{h}})^{1/2}$.

The mean distance $\langle x\rangle$ of the beam to a beam propagating without any displacement is given by

$$\langle x(\Delta\Theta_m)\rangle = \int I_0(\Delta\Theta - \Delta\Theta_m)\{x_1|D_{01}|^2 + x_2|D_{02}|^2\}\,\mathrm{d}(\Delta\Theta) / \int I_0(\Delta\Theta - \Delta\Theta_m)\{|D_{01}|^2 + |D_{02}|^2\}\,\mathrm{d}(\Delta\Theta),$$

where x_1, x_2, D_{01} and D_{02} are functions of $\Delta\Theta$.

All the formulae depend on the parameter η which, for a given value of the offset, is different for σ and π polarizations. At the entrance of the crystal the wave is linearly polarized, the polarization vector being inclined by the angle $\psi \simeq 45^\circ$ with respect to the plane of diffraction. This means that the intensity is half σ and half π and this has been taken into account.

The theoretical curves for $\langle x(\Delta\Theta_m)\rangle$ have been calculated for different values of the FWHM of the Gaussian angular distribution and fitted to the experimental points shown in Fig. 7, as explained in the previous section. The best fit (shown with a full curve in Fig. 7) is obtained for a Gaussian angular distribution whose FWHM is equal to 75 arcsec, in good agreement with the divergence deduced by alternative methods in previous experiments.

The good agreement between this calculation and the experimental points in Fig. 7 demonstrates that the residual signal in the XMCD spectra, proportional to the derivative of the absorption spectra, is indeed originated by a lateral displacement of the beam when it crosses the QWP, which varies with $\Delta\Theta$.

6. Conclusions

The residual signal superimposed on the XMCD spectra when the polarization helicity is switched from right to left by means of a QWP has been systematically studied.

This is interpreted as originating from three different effects. First, the expected variation of the transmission by a perfect crystal as a function of the offset induces a non-zero signal constant along the spectrum. Second, the defects present in the diamond plate may generate a variation of transmission along the plate and therefore a non-constant signal along the spectrum. The third effect originates from the lateral displacement of the beam when propagating in the QWP and gives rise to a signal which is proportional to the derivative of the absorption of the sample. This displacement depends on the offset and can be well understood qualitatively by considering the X-ray propagation inside the Borrmann fan in a perfect crystal. In the symmetric case, for example, at exact Bragg incidence both wavefields propagate along the reflecting planes. For a non-zero offset the two wavefields propagate symmetrically

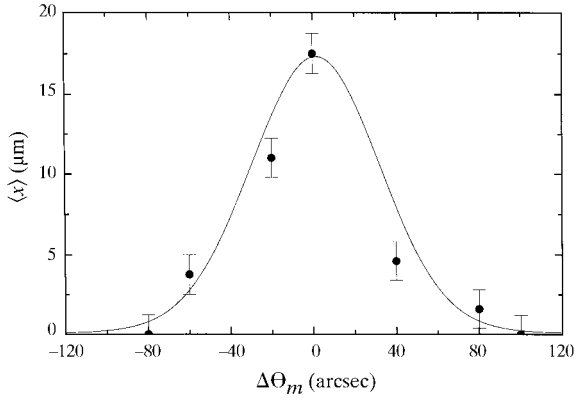

Figure 7
Mean lateral displacement ($\langle x\rangle$) of the beam calculated by X-ray dynamical theory considering a Gaussian angular distribution of the incident beam with FWHM of 75 arcsec (full line). The filled circles correspond to the displacements of the beam deduced from experiments.

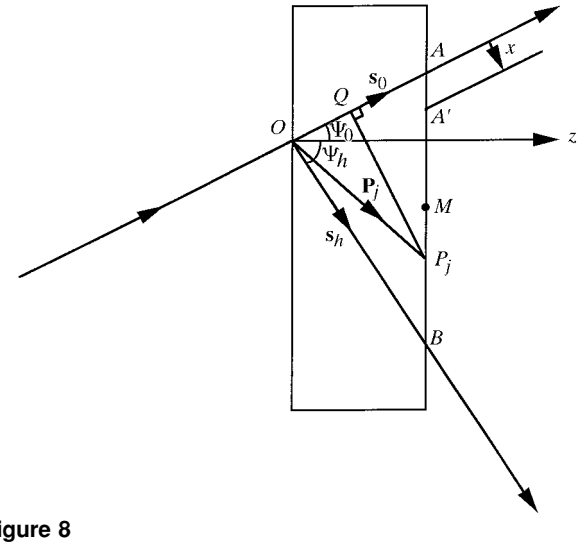

Figure 8
Geometrical construction in direct space of the propagation direction of the Poynting vector $\mathbf{P}_j$ in the asymmetric Laue case. OAB is the Borrmann fan. A' is the mean position of a beam giving rise to a forward-diffracted beam whose distance to the incident beam is x.

with respect to the reflecting planes but with different intensities. For a large offset only one wavefield carries all the intensity and this wavefield propagates almost along the incident direction. Consequently, for a large offset there is no lateral displacement and, if the incident beam was a plane wave, the normal operating conditions (large offsets) would not give rise to any noticeable displacement of the beam. A displacement was clearly evidenced at the offset of 40 arcsec for example (about eight times the Darwin width) due to the quite large size of the DCI source which generates a Gaussian angular distribution with a FWHM of the order of 75 arcsec.

With third-generation sources like the ESRF where recent experiments performed on beamline ID24 have shown that the FWHM of the incident angular distribution is of the order of 4.5 arcsec (Pizzini *et al.*, 1998), the displacement of the beam at large offsets almost vanishes. However, the residual signal shown in Pizzini *et al.* (1998) still contains a small modulation around the absorption edge which cannot be described by a derivative signal. This modulation could be due to the defects present in the available diamond plates which could give rise to a small misorientation of the emerging beam, impossible to model. Such an effect would be negligible in the experiments reported here but can be a small contribution in the residual signal shown in Fig. 1.

In summary, accurate XMCD measurements with tunable polarization helicity using a non-perfect quarter-wave plate require the subtraction of the residual signal.

One of us (CG) acknowledges financial support from FAPESP (contract number 96/05586-6), CNPq and PRONEX.

References

Authier, A. (1961). *Bull. Soc. Fr. Mineral. Cristallogr.* **84**, 51–89.
Authier, A. (1986). *Acta Cryst.* A**42**, 414–426.
Bergevin, F. de & Brunel, M. (1972). *Phys. Lett.* A**39**, 141–142.
Chen, C. T., Sette, F., Ma, Y., Modesti, S. & Smith, N. V. (1990). *Phys Rev. B*, **42**, 7262–7265.
Dartyge, E., Fontaine, A., Baudelet, F., Giorgetti, C., Pizzini, S. & Tolentino, H. (1992). *J. Phys. I (Paris)*, **2**, 1233–1255.
Dmitrienko, V. E. & Belyakov, V. A. (1980). *Sov. Tech. Phys. Lett.* **6**, 621–622.
Gibbs, D., Harshman, D. R., Isaacs, E. D., McWhan, D. B., Mills, D. & Vettier, C. (1988). *Phys. Rev. Lett.* **61**, 1241–1244.
Giles, C. (1995). PhD thesis, Université Paris 7, France.
Giles, C., Malgrange, C., Goulon, J., de Bergevin, F., Vettier, C., Dartyge, E., Fontaine, A., Giorgetti, C. & Pizzini, S. (1994). *J. Appl. Cryst.* **27**, 232–240.
Giles, C., Malgrange, C., Goulon, J., de Bergevin, F., Vettier, C., Fontaine, A., Dartyge, E. & Pizzini, S. (1994). *Nucl. Instrum. Methods*, A**349**, 622–625.
Giles, C., Malgrange, C., Goulon, J., Vettier, C., de Bergevin, F., Freund, A., Elleaume, P., Dartyge, E., Fontaine, A., Giorgetti, C. & Pizzini, S. (1993). *Proc. SPIE*, **2010**, 136–149.
Hirano, K., Izumi, K., Ishikawa, T., Annaka, S. & Kikuta, S. (1991). *Jpn. J. Appl. Phys.* **30**, L407–410.
Malgrange, C. (1996). *X-ray and Neutron Dynamical Diffraction: Theory and Applications*, edited by A. Authier, S. Lagomarsino & B. K. Tanner, *NATO ASI Ser., Ser. B: Physics*, No. 357, pp. 91–109. New York/London: Plenum Press.
Pizzini, S., Bonfim, M., Baudelet, F., Tolentino, H., San Miguel, A., Mackay, K., Malgrange, C., Hagelstein, M. & Fontaine, A. (1998). *J. Synchrotron Rad.* **5**, 1298–1303.
Pizzini, S., Fontaine, A., Garcia, L. M., Bobo, J.-F., Piecuch, M., Baudelet, F., Malgrange, C., Alimoussa, A., Snoeck, E. & Casanove, M. J. (1997). *J. Magn. Magn. Mater.* **166**, 38–44.
Schütz, G., Frahm, R., Mautner, P., Wienke, R., Wagner, W., Wilhelm, W. & Kienle, P. (1989). *Phys. Rev. Lett.* **62**, 2620–2623.
Tolentino, H., Dartyge, E., Fontaine, A. & Tourillon, G. (1988). *J. Appl. Cryst.* **21**, 15–21.
Vettier, C. (1994). *J. Magn. Magn. Mater.* **129**, 59.